Biochimica et Biophysica Acta 1828 (2013) 461–470

Contents lists available at SciVerse ScienceDirect

Biochimica et Biophysica Acta

journal homepage: www.elsevier.com/locate/bbamem

The effect of extracellular conductivity on electroporation-mediated molecular delivery

Jianbo Li [a], Wenchang Tan [b], Miao Yu [a], Hao Lin [a,*]

[a] Mechanical and Aerospace Engineering, Rutgers, The State University of New Jersey, 98 Brett Road, Piscataway, NJ 08854, USA
[b] State Key Laboratory for Turbulence and Complex Systems, Department of Mechanics and Engineering Science, College of Engineering, Peking University, Beijing 100871, China

ARTICLE INFO

Article history:
Received 15 February 2012
Received in revised form 3 August 2012
Accepted 20 August 2012
Available online 27 August 2012

Keywords:
Electroporation
Electropermeabilization
Electrophoresis
Molecular delivery
Electrical conductivity
Field amplified sample stacking

ABSTRACT

In this work, the effect of extra-cellular conductivity on electroporation-mediated molecular delivery efficiency is investigated. A numerical model combining the Smoluchowski equation for membrane permeabilization and the Nernst–Planck equations for ion transport is used to simulate the evolution of ion concentration spatially and temporally. The results are compared with and used to interpret trends observed from previous experimental measurements. Agreements are found which suggest the critical importance of electrophoretic transport. This mechanism controls delivery efficiency on the quantitative level. Meanwhile, a simple formula is developed to predict the molecular content delivered via electrophoresis. The formula can be used as a compact model which provides good approximation to the full numerical model while avoiding the computational cost.

1. Introduction

Electroporation is a well-known mechanism to deliver biologically active molecules into the cell cytoplasm [1,2]. The technique finds broad applications in areas such as cell transfection, protein insertion, gene and cancer therapy, stem-cell research, among many others [1–11]. The process is complex and involves two major aspects: the permeabilization of the cell membrane via an applied electric field [12–14], and the molecular transport into the permeabilized cells (molecular uptake). A relatively mature understanding has been developed for the first aspect. The permeabilization results from the formation of aqueous, conducting pores on the membrane [15–23], and a Smoluchowski equation (SE) is often used to statistically describe the dynamics of the pore population [24–34]. The second aspect, on the other hand, still eludes a comprehensive understanding, although past work provided key insights into the underlying physical mechanisms. In general, large molecules such as DNA, RNA, and protein behave in a manner more complex than small ions such as calcium and propidium iodide (PI) [35–37], and endocytosis, electrophoresis, and diffusion may all contribute to transport [38–43,36,44–46]. Further identification of these specific mechanisms is important in developing a prediction capability for this important phenomenon.

This work focuses on investigating the delivery of small molecules via electroporation. We are motivated by experimental observations from previous research, namely, by Zimmermann and co-authors in two companion papers [47,48]. In these experiments, the delivery of PI into murine myeloma cells was investigated under both classical [47] and supra-electroporation [48] conditions, and an inverse correlation between the percentage of PI uptake (or total amount of delivery) and the extracellular conductivity was discovered. Although several possible mechanisms have been proposed by the authors [47–49], a causal relation between them and the data trends has yet to be established.

We propose that the electrophoretic transport of the target ions is largely responsible for the observed conductivity effects. We follow our previous work where we have established a model framework to track the delivery of small ions into electropermeabilized cells [50]. We combined an asymptotic Smoluchowski equation (ASE) for membrane permeabilization with a Nernst–Planck (NP) equation system for ion transport, and simulated calcium ion entry into Chinese Hamster Ovary cells. In contrast to the previous compartment or simplified diffusion models [51–57], we simulate the spatial and temporal evolution of both the pore statistics and the molecular concentration of the pertinent molecules. Our results compared well with experimental data from [58], and revealed that electrophoresis plays an important role in molecular transport. Furthermore, we found that field-amplified sample stacking (FASS), an electrokinetic mechanism arising from the presence of a gradient in the electrophoretic velocity, determines the achievable molecular concentration within the cell. Because the latter is reciprocally correlated with the extracellular electrical conductivity, the finding motivates us to

* Corresponding author. Tel.: +1 732 445 2322; fax: +1 732 445 3124.
E-mail address: hlin@jove.rutgers.edu (H. Lin).

0005-2736/$ – see front matter © 2012 Elsevier B.V. All rights reserved.
http://dx.doi.org/10.1016/j.bbamem.2012.08.014

pursue an interpretation of the data trends from [47,48], with the objective to identify the underlying physical mechanisms.

We will use the model developed in [50] to study the entry of PI into murine myeloma cells, using experimental parameters found in [47,48]. We emphasize that the focus of this work is not to improve the efficiency of these particular electroporation schemes, but to provide general mechanistic interpretations to the behavior of a complex system. The major contribution lies in the development toward a prediction capability of this broadly useful technique. In Section 2, the formulation and simulation method are briefly outlined. In Section 3.1, we use simulation to investigate membrane permeabilization and PI delivery with nano-second pulses, and compare the results with those from [48]. Our results indicate that only a weak correlation exists between the degree of permeabilization and the extracellular conductivity. In Section 3.2, a compact formula is developed to approximate results predicted by the full model, and is subsequently used to analyze the data trends from both [47] and [48]. For both cases, the simulation and the compact formula produce an expected inverse correlation between delivery and conductivity, which is compared in detail with the experimental data. The results reveal good agreement, suggesting that electrophoresis may be the root cause of the observed trends. On the other hand, quantitative discrepancies still exist between the prediction and the data, which points toward mechanisms not included in the present model. In Section 4, several possible effects including those of charging time, electrodeformation forces, and diffusion are addressed. We draw our conclusions in Section 5.

2. Model formulation

2.1. The electric problem

The overall model formulation follows our previous work [50]. A schematic of the problem is shown in Fig. 1. The cell is idealized to be a thin, rigid, and spherical shell of radius a, and a spherical coordinate system is adopted. The x-axis is chosen to align with the direction of the applied electric field. σ and Φ denote the electrical conductivity and electric potential, and the subscripts i and e denote intra- and extra-cellular, respectively. This single-cell-level treatment is a good approximation to a cell in suspension when the suspension is dilute enough such that the interference between the cells is negligible. The intra- and extra-cellular electric potentials are governed by the Ohmic equation:

$$\nabla\cdot\sigma_i\nabla\Phi_i = 0, \nabla\cdot\sigma_e\nabla\Phi_e = 0. \tag{1}$$

Note that we have neglected the displacement current in the electrolytic solutions by assuming instantaneous charge relaxation. These equations are respectively solved, and coupled on the membrane through the electric current continuity condition,

$$-\mathbf{n}\cdot\sigma_i\nabla\Phi_i = -\mathbf{n}\cdot\sigma_e\nabla\Phi_e = C_m\frac{\partial V_m}{\partial t} + g_l(V_m - V_{\text{rest}}) + \sum_{j=1}^{K(t,\theta)} i_p\left(R_j(t,\theta), V_m\right)/\Delta A, \tag{2}$$

where $\mathbf{n}$ is the local unit normal vector on the membrane, C_m is the membrane capacitance, g_l is the leakage conductance, and V_m (defined as $(\Phi_i - \Phi_e)_{r=a}$) and V_{rest} are the transmembrane and the rest potential, respectively. In what follows, we abbreviate the transmembrane potential as TMP. The three terms on the right-hand side of Eq. (2) respectively indicate the three currents through the membrane: the displacement current, the leakage current across the intact cell membrane, and the ionic current through the pores at a specific location. In the last term, ΔA is a local area element, K is the total number of pores on the element, and i_p is the current through an individual pore with radius R_j. i_p is given by the formula

$$i_p = \frac{2\pi R_j^2\sigma_{\text{eff}}V_m}{\pi R_j + 2h}, \tag{3}$$

where $\sigma_{\text{eff}} = (\sigma_e - \sigma_i)/\ln(\sigma_e/\sigma_i)$ is an effective pore conductivity, and h is the membrane thickness. Eq. (3) is obtained by directly solving the Nernst–Planck equations for a binary electrolyte solution around a cylindrical, membrane-bound pore. Detailed derivations can be found in our previous work [59].

2.2. Pore nucleation and evolution

The ASE model describing the nucleation and evolution of the pore population follows that by Krassowska and Filev [33],

$$\frac{dN}{dt} = \alpha e^{\left(V_m/V_{ep}\right)^2}\left(1 - \frac{N}{N_0 e^{q\left(V_m/V_{ep}\right)^2}}\right), \tag{4}$$

$$\frac{dR_j}{dt} = U\left(R_j, V_m, \tau\right), j = 1, 2, \cdots, k. \tag{5}$$

Here $N(t,\theta)$ is the local pore number density, α, N_0, q, and V_{ep} are constants, U is the advection velocity, and τ is an effective membrane tension. According to this model, pores nucleate at an initial radius, $R_* = 0.51$ nm, and at a rate described by Eq. (4). They then evolve in size according to Eq. (5), to minimize the total energy of the lipid membrane. Resealing effects are also captured by the ASE. Further details of the model, as well as relevant parameters are found in [33], and are not presented here for brevity.

2.3. Species transport

We adopt a generalized NP system to simulate species transport. In the following, we consider three specific species, free PI ions (denoted by PI^{2+}), DNA and RNA binding sites (denoted by B), and bound PI (denoted by PI − B). We assume that the binding sites are uniformly distributed inside the cell with a molar concentration of

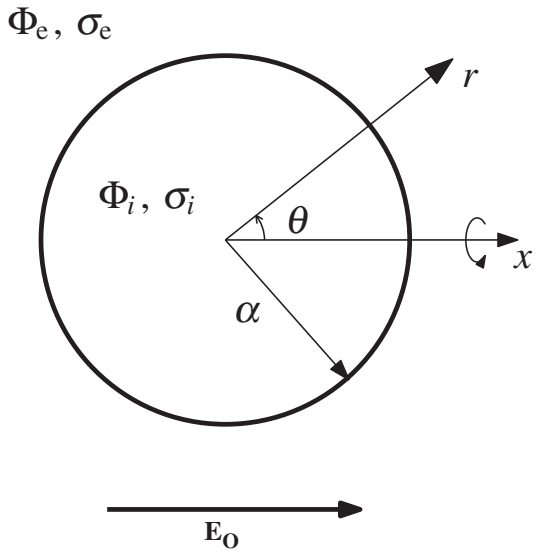

Fig. 1. Schematic of the problem. The x-axis is aligned with the direction of the electric field. r denotes the radial position, and θ is the inclination angle. The problem is axisymmetric with respect to the x-axis.

$[B]_{i,o}$, where the subscript i again denotes intracellular, and o denotes an initial value. The extracellular PI^{2+} concentration is $[PI^{2+}]_{e,o}$ (Table 1). When free PI ions enter the cell through the permeabilized membrane, they bind to DNA and RNA molecules at the binding sites. Upon excitation the complex emits fluorescent signal which is observed by microscopy. The reaction is described by

$$PI_i^{2+} + B_i \underset{k_-}{\overset{k_+}{\rightleftharpoons}} PI{-}B_i,$$

where k_+ and k_- are the association and dissociation rate constants, respectively. The NP equations are modified with production terms to capture this process:

$$\frac{\partial\left[PI^{2+}\right]}{\partial t} = \nabla\cdot\left(wFz\left[PI^{2+}\right]\nabla\Phi\right) + \nabla\cdot D\nabla\left[PI^{2+}\right] - k_+[B]\left[PI^{2+}\right] + k_-[PI{-}B], \tag{6}$$

$$\frac{\partial[B]}{\partial t} = -k_+[B]\left[PI^{2+}\right] + k_-[PI{-}B], \tag{7}$$

$$\frac{\partial[PI{-}B]}{\partial t} = k_+[B]\left[PI^{2+}\right] - k_-[PI{-}B]. \tag{8}$$

Here $\left[PI^{2+}\right]$, [B], and [PI − B] denote the molar concentrations, F is the Faraday constant, and z, D, and w are the valence number, diffusion coefficient, and the mechanical mobility of PI^{2+}, respectively. Because in general DNA and RNA have very low mobility within the cell, they are assumed to be fixed. Eqs. (6)–(8) are solved for both the intra- and extra-cellular spaces, and are coupled on the membrane by continuity of the molar flux density for PI^{2+}:

$$\mathcal{F}_{i,e} = \mathcal{F}_m, \tag{9}$$

where,

$$\mathcal{F}_{i,e} \equiv -\mathbf{n}\cdot\left(wFz\left[PI^{2+}\right]\nabla\Phi + D\nabla\left[PI^{2+}\right]\right)_{i,e}, \tag{10}$$

$$\mathcal{F}_m \equiv \rho_p \frac{D(Pe + \ln(\gamma))}{h}\frac{(\gamma-1)}{\ln\gamma}\frac{\left(\left[PI^{2+}\right]_e - \left[PI^{2+}\right]_i \exp(Pe)\right)}{(1-\gamma\exp(Pe))}. \tag{11}$$

Table 1
List of model parameters.

Symbol	Definition	Value
a	Cell radius	7 μm [47,48]
h	Membrane thickness	5 nm
σ_e	Extracellular conductivity	0.08–0.5 S/m [47,48]
σ_i	Intracellular conductivity	0.4 S/m [47,48]
F	Faraday constant	96,485 C/mol
R	Universal gas constant	8.314 J/K·mol
T	Room temperature	298.15 K
k_+	Association rate constant	1.54 $(\mu MS)^{-1}$ [60,61]
k_-	Dissociation rate constant	5.17 s^{-1} [60,61]
D_e	Diffusivity of PI^{2+} in the extracellular solution	437 $\mu m^2/s$[a]
D_i	Diffusivity of PI^{2+} in the cytoplasm	146 $\mu m^2/s$[b]
z	Valence number for PI^{2+}	+2
$\left[PI^{2+}\right]_{e,o}$	Initial PI^{2+} concentration in the extracellular solution	37.4 μM [47,48]
$[B]_{i,o}$	Initial binding site concentration in the cytoplasm	6.93 mM [47,60]

[a] Direct measurement, courtesy of M. M. Sadik.
[b] This value is taken to be one-third of D_e. The reduction of the diffusivity of PI^{2+} within the cell is assumed to follow the same ratio as Ca^{2+} [50].

Here $\mathcal{F}_{i,e}$ are the flux densities of $[PI^{2+}]$ from the intra- and extra-cellular spaces, respectively, $\mathcal{F}_m$ is the flux density across the membrane, $Pe \equiv wFzV_m/D$ is an effective Péclet number, and $\gamma = \sigma_i/\sigma_e$ is the intra- to-extra-cellular conductivity ratio. Eq. (11) is derived assuming that the sum of the electrophoretic and diffusive fluxes is constant along the axis within the pore, and a detailed derivation is found in [50]. Note that when $V_m = 0$, Eq. (11) is reduced such that it includes the diffusive flux only. Eqs. (6)–(11) are coupled to (1)–(5) through two variables, Φ and ρ_p. The latter is calculated for every area element after the pore statistics is obtained,

$$\rho_p(t,\theta) = \sum_{j=1}^{K(t,\theta)} \pi R_j^2/\Delta A.$$

This quantity is the local fractional "opening" area occupied by the pores, and is a measure of membrane permeabilization. Following [50], we name it the "pore area density" (PAD).

2.4. Numerical implementation

Eqs. (1)–(9) are solved numerically using a finite volume, alternative direction implicit (ADI) scheme. The problem is effectively two-dimensional as we assume axisymmetry about the x-axis. For initial conditions, we assume

$$N(0,\theta) = 0, \Phi_i(0,r,\theta) = V_{\text{rest}}, \Phi_e(0,r,\theta) = 0.$$

The initial concentrations for free PI^{2+} and intracellular DNA/RNA binding sites are given in Table 1. The simulation domain is a large sphere $20a$ in radius. On the outer boundary, we prescribe

$$\Phi_e(t, r = 20a, \theta) = -E_0 r\cos\theta,$$

where E_0 is the strength of the applied field. This prescription well-approximates the ambient condition of a uniform electric field. A non-uniform spherical grid with higher resolution around the membrane is adopted to optimize computational efficiency. The numerical convergence is tested with respect to resolution by increasing the number of grids. All general parameters pertinent to the permeabilization model (1–5) are taken from [33], and are not repeated here for brevity. Parameters specific to this study (e.g., $\sigma_{i,e}$, a, and E_0), and the rate constants are summarized in Table 1. They are specified to best approximate the experimental conditions in [47,48]. Note that the above model is derived assuming the pores are cylindrical in shape. This is only an idealization of the realistic pore shape. The pores are in general believed to have no edges, and molecular simulation suggests they may even have irregular shapes [17].

3. Results

We first present simulated results on cell permeabilization and PI delivery under supra-electroporation conditions, and compare with experimental data from [48] (Section 3.1). In Section 3.2, we develop a compact formula to interpret the predicted and observed trends, and use it to further correlate with experimental data under classical electroporation conditions from [47].

3.1. Simulation of supra-electroporation with varying extracellular conductivity

Fig. 2 shows the permeabilization of a cell membrane under a 160 kV/cm electric pulse 95 ns in length. In Fig. 2a, the evolution of the TMP as a function of time at the anode-facing pole ($\theta = \pi$) is shown, for the various extracellular conductivities ($\sigma_e = 0.1$–0.5 S/m). All cases exhibit an initial increase in the magnitude of the potential, followed by a subsequent decrease due to the permeabilization of

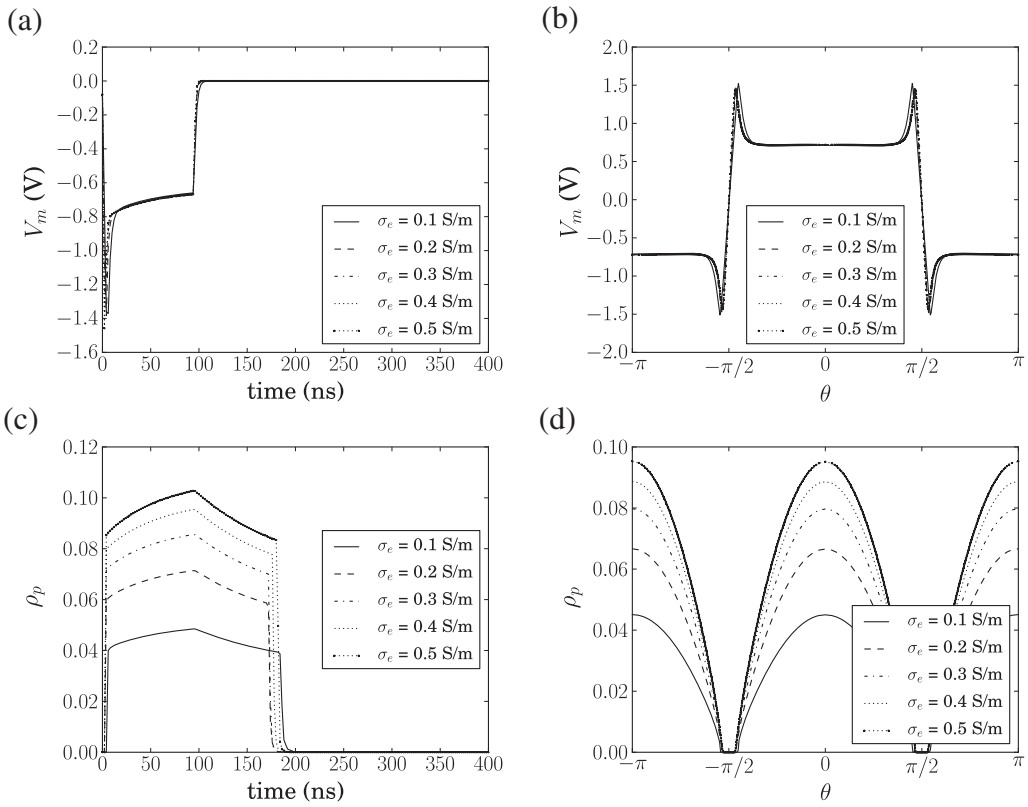

Fig. 2. Membrane permeabilization under a 160 kV/cm pulse 95 ns in length, for various extracellular conductivities (0.1–0.5 S/m). (a) The development of the TMP, V_m, at the anode-facing pole ($\theta=\pi$). (b) The distribution of the TMP as a function of the position along the membrane (θ) at $t=95$ ns. (c) The development of the PAD, ρ_p, at the anode-facing pole ($\theta=\pi$). (d) The distribution of the PAD as a function of θ at $t=95$ ns.

the cell membrane. The permeabilization increases the effective conductivity of the membrane caps, such that further growth in the TMP is limited. After the pulse ceases at 95 ns, the TMP drops to near-zero. Fig. 2b shows the distribution of the TMP along the membrane at $t=95$ ns. In Fig. 2c, we plot the evolution of the PAD (ρ_p) as a function of time, also at the anode-facing pole ($\theta=\pi$). Consistent with the behavior of V_m, the increase in ρ_p goes through a rapid stage followed by a slower one. The pores begin to shrink immediately after the pulse ceases, and the majority of them vanish between 180 and 200 ns. In Fig. 2d, ρ_p is plotted as a function of θ at the end of the 95-ns-long pulse.

The salient feature of Fig. 2 is that both the TMP and PAD are insensitive to the extracellular conductivity. (The intracellular conductivity is considered to be a constant at $\sigma_i=0.4$ S/m.) This insensitivity can be explained by the interdependence of the TMP and the PAD in the model framework. According to Eqs. (4) and (5), the PAD exponentially depends on the square of the TMP. On the other hand, the TMP has an approximate linear dependence on the PAD through Eq. (2). As a result, a small increase in the TMP leads to a great increase in the PAD, which in turn limits further growth of the former parameter. This dynamic process leads to a final equilibration for both ρ_p and V_m, and the equilibrium values depend only weakly on σ_e. The result suggests that within the validity of the current model framework, the strong dependence of molecular delivery on the extracellular conductivity is not explained by the variations in permeabilization.

We remark that when compared with results for classical electroporation ($E_0\sim1$ kV/cm) [50], the permeabilized areas at the anode- and cathode-facing caps are larger. In addition, the maximum PAD is 1–2 orders greater than that in the classical cases. However, these results are consistent with model predictions by other authors for supra-electroporation [31,34].

Next we present results for PI delivery into the permeabilized cell, also for $E_0=160$ kV/cm and a pulse length of $t_{pulse}=95$ ns. For the exemplary results shown in Fig. 3, $\sigma_e=0.1$ S/m. The concentrations for the dye in free ($[PI^{2+}]$) and bound ($[PI-B]$) forms are plotted along the cell centerline (the x-axis). Due to the small time scale involved, both exhibit very narrow peaks inside the cell immediately next to the anode-facing cap ($x=-a=-7$ μm, Fig. 3a, b). An enlarged view in Fig. 3c and d shows more details of the development. In Fig. 3c, the free-PI concentration reaches a peak value around 0.43 mM by the end of the pulse, mediated mainly by electrophoretic transport. This peak value is much higher than the basal extracellular concentration, $\left[PI^{2+}\right]_{e,o}=37.4$ μM. This concentration enhancement is caused by a difference in the electrophoretic velocity across the cell membrane as we have previously demonstrated, and is termed field-amplified sample stacking (FASS) [50]. After the pulse ceases, the concentration slowly diffuses away, during which we also observe leakage through the permeabilized membrane. On the contrary, the concentration for bound PI continues to increase even after the pulse, due to continuous binding of the free ions with the available sites. (Note the binding time scale is ~0.1 ms, much longer than the time scale presented. Such a long binding time may lead to delayed observation of the fluorescence signal such as the nano-second electroporation experiments in [62].)

In Fig. 4, the time course of total PI delivery is examined for the various conductivities studied in [48]. The total delivered molecular content within the cell, PI_{tot}, is calculated by summing that of both the free and bound PI. The total delivery first increases linearly with time until the pulse ends at 95 ns, indicating the dominant role of electrophoresis. After the pulse ceases, noticeable leakage is observed, especially for the lower conductivity cases where the intracellular specific concentrations are higher due to FASS. PI_{tot} eventually reaches equilibrium values, and after 400 ns no significant changes are observed. For these cases, diffusion does not contribute appreciably to the total delivery, mainly due to the rapid decrease in ρ_p after

the pulse ends (see Fig. 2c). Further discussions on the role of diffusion are found in Section 4.

In Fig. 5a and b, the simulated total PI delivery at $t = 800$ ns is examined and shown as symbols, for the parametric configurations studied in [48]. (The dashed-lines are calculated with a compact model (12) which is presented in Section 3.2.) In Fig. 5a, the total PI is plotted as a function of the applied field strength, E_0, and for the various extracellular conductivities, σ_e. The pulse length is 95 ns. In Fig. 5b, a single field strength, $E_0 = 160$ kV/cm is chosen, and the effects of pulse length (11–95 ns) are studied. For comparison, the experimental results from [48] are adapted and presented in Fig. 5c and d. Very good agreements are observed in the general data trends. First, PI uptake depends linearly on the field strength (Fig. 5a and c), and the slope of the linear curves decreases with an increasing conductivity. Second, the total delivery shows an inverse correlation with the extracellular conductivity (Fig. 5b and d), and the correlation is stronger with longer pulses. These agreements suggest that transport, and in particular via electrophoresis, plays a key role in mediating the delivery and producing the results shown. The mechanism is further analyzed with a simplified understanding below.

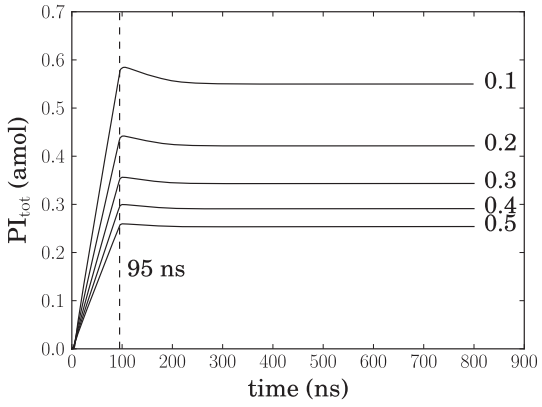

Fig. 4. The time course of simulated total PI content (PI_{tot}). $E_0 = 160$ kV/cm and $t_{pulse} = 95$ ns. The numbers 1–5 denote σ_e in the unit of S/m.

3.2. A compact model and comparison with classical electroporation

The behavior observed in Fig. 5 can be understood with a simplified model. In Appendix A and via a control volume analysis, we show that the total molecular delivery, c_{tot}, can be approximated by the following formula,

$$c_{tot} = t_{pulse} \times \left[c_e w F z E_o \pi a^2 \left(\frac{3\sigma_i}{2\sigma_e + \sigma_i} \right) \right]. \quad (12)$$

Here c_e is the extracellular concentration of the target molecule. The simple theory temporarily ignores diffusion and takes into account only the electrophoresis transport, and the term within the square brackets represents the total electrophoretic flux into the cell. The calculated results using the same parameters as in the previous section are shown as dashed lines in Fig. 5a and b. The simple formula provides a good approximation when compared with the results from the full model. The agreement suggests that indeed electrophoresis is the main mode of molecular transport for the cases studied, and that Eq. (12) can be used as a compact, convenient formula in place of the more complex and costly full-model simulations.

More importantly, Eq. (12) correctly captures the linear dependence of c_{tot} on E_0, as well as its inverse dependence on σ_e. The former is simply due to the linear dependence of the electrophoretic velocity

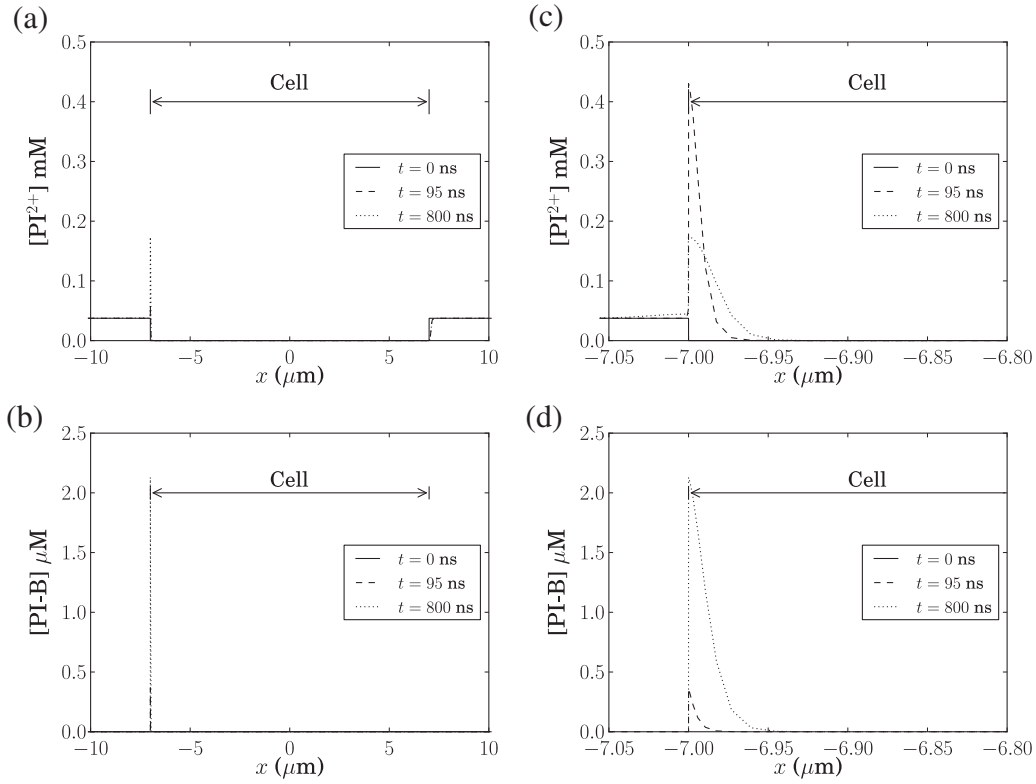

Fig. 3. Concentration evolution for free and bound PI along the cell centerline (x-axis) for $E_0 = 160$ kV/cm, $t_{pulse} = 95$ ns, and $\sigma_e = 0.1$ S/m. The cell extends from $x = -7$ to 7 μm. (c) and (d) zoom in around the anode-facing pole ($x = -7$ μm) to demonstrate detailed profile evolution.

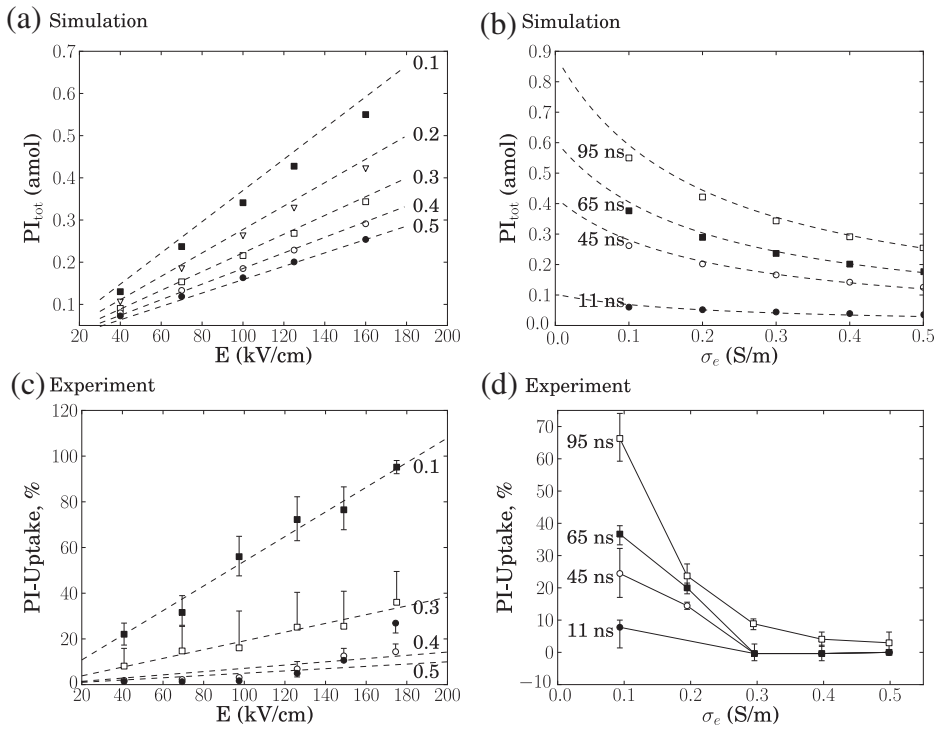

Fig. 5. Simulated total PI delivery and comparison with experimental data. (a) Simulated total PI content within the cell (PI_{tot}, symbols) for $t_{pulse}=95$ ns, as a function of the applied field strength, E_0, and the extracellular conductivity, σ_e. The numbers 1–5 denote σ_e in the unit of S/m. (b) Simulated PI_{tot} (symbols) as a function of σ_e and t_{pulse} for $E_0=160$ kV/cm. For both (a) and (b), the dashed lines are theoretical predictions generated with Eq. (12). (c) and (d): experimental data adapted from Fig. 3 in [48]. The dashed lines in (c) are least-square linear fits. Please note that the *y* labels in (c) and (d), "PI-Uptake, %", mean the percentage of successful delivered cells.

on the field strength, and the latter is due to the heterogeneous spatial distribution of the electric field, which depends on both the intra- and extra-cellular conductivities. (See Appendix A for the detailed derivation.) The functional dependence reveals that

$$c_{tot}\sim\frac{3\sigma_i}{2\sigma_e+\sigma_i}, \tag{13}$$

where σ_i is assumed to depend only on the cell type, and is a fixed constant for all cases studied.

The availability of Eq. (12) allows us to further analyze the data trends observed in the experiments. Note that a direct comparison with the results from [48] is not possible, because our model predicts the total delivery into a single cell, whereas the experimental data measures the percentage of cells with successful PI uptake. Instead, we attempt to fit the experimental data with Eq. (13). In Fig. 6, the black dots are the slopes extracted from the least-square linear fits from Fig. 5c. The dashed curve is a least-square fit assuming a functional form of $A[3\sigma_i/(2\sigma_e+\sigma_i)]$, where $A=0.20$ is the resulting fit parameter. This fit captures the trend, but tends to produce a somewhat weaker dependence on σ_e when compared with the data. However, a correction of the functional form with an added constant produces an excellent agreement,

$$f_2(\sigma_e)=B\left(\frac{3\sigma_i}{2\sigma_e+\sigma_i}+C\right), \tag{14}$$

where $B=0.44$, $C=-1.28$ are determined to minimize the fitting error. The resulting curve is shown in Fig. 6a as a dot-dashed line.

Eq. (12) also permits us to conveniently analyze the other data, namely, the experimental measurements by Djuzenova et al. [47]. This work proceeds [48], and investigates the effect of extracellular conductivity with classical ($E_0=3$ kV/cm and the field exponentially decays with a time constant of 40 μs) instead of supra-electroporation. The

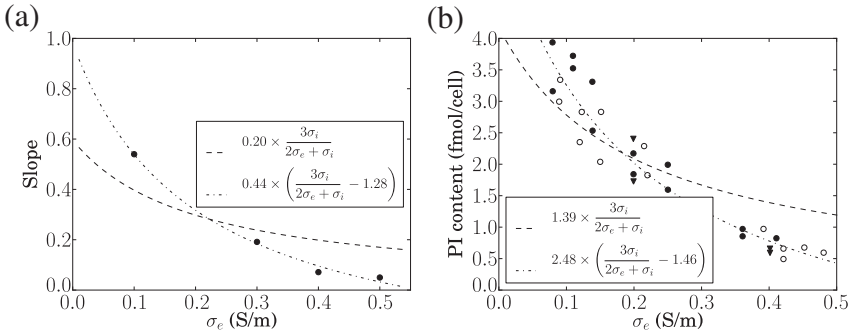

Fig. 6. Parametric fitting of the experimental data on PI delivery. In (a), the dots are the numerical values of the slopes extracted from the linear fits in Fig. 5c. In (b), the experimental data are regenerated from Fig. 3 in [47], where open circles, solid circles, and triangles represent KCl, NaCl, and Na_2SO_4 solutions, respectively. For both cases, the dashed curves are fits with the original functional form (13). The dot-dashed are fits from the modified functional form (14).

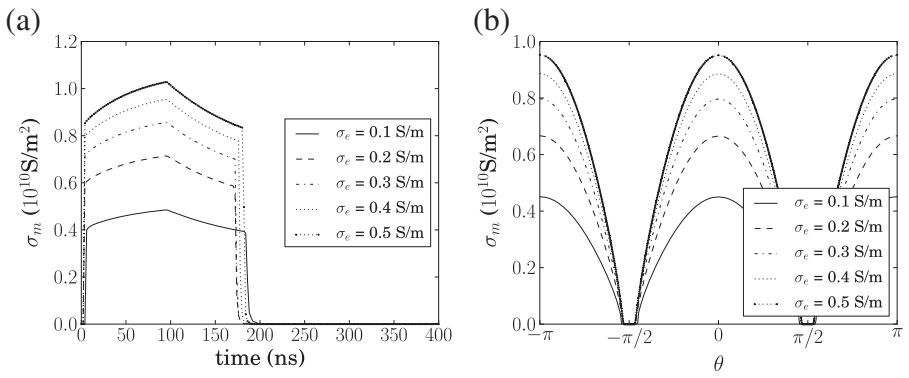

Fig. 7. Calculated membrane conductance (σ_m) as a function of extracellular conductivity. The membrane conductance is consistently higher as the extracellular conductivity increases. In (a), the conductance is shown at $\theta=\pi$ and as a function of time. In (b), it is shown as a function of θ at $t=95$ ns.

experimental configuration is otherwise similar to [48]. The data is adapted and presented in Fig. 6b as symbols. Same as in the previous case, we use Eq. (13) to fit the data (dashed), and the result reveals a weaker dependence on σ_e. On the other hand, fitting with the modified form Eq. (14) (dot-dashed) yields a satisfactory curve which well-captures the trends. Interestingly, the fit constant C for the two cases in Fig. 6 closely matches each other (-1.28 and -1.46, respectively), pointing toward a consistent functional form, although the pulsing schemes are drastically different.

The results presented above lead to two important speculations. First, the formula (12) as well as the full model captures an essential part of the physical processes involved. While quantitatively discrepancies are present, qualitatively the trends are reproduced. It is particularly interesting to see that a simple modification based on the prediction agrees satisfactorily with the correlations observed in both [47] and [48]. Based on this result, we believe that electrophoretic ion transport plays a significant role in mediating the delivery of small charged molecules. Second, an unknown mechanism not included in our model also contributes to delivery, which is evidenced by the constant C that is artificially added to Eq. (14). We are currently investigating various possibilities for this discrepancy. Regardless of its nature and origin, our results indicate that the effect is also linearly proportional to the applied field strength.

4. Discussion

The current work posits that the molecular uptake dependence on extracellular conductivity is mediated by electrophoretic transport. However, the mechanism we propose is not necessarily exclusive. For a complex process as such, multiple mechanisms may simultaneously contribute to the system behavior, and some possibilities are discussed below.

4.1. Membrane and electrode charging times

The charging time is the most obvious conductivity-dependent parameter in an electroporation system. In Djuzenova et al. [47], the membrane charging process as a possible contributor has been discussed. The relaxation time, τ_m, for a near-insulating membrane is given by

$$\tau_{\text{charg}} = aC_m\left(\frac{1}{\sigma_i}+\frac{1}{2\sigma_e}\right),$$

which shows an inverse dependence on σ_e. However, as the authors argued in [47], this dependence would rather produce an opposite trend. According to the formula, a decreasing σ_e leads to an increasing charging time. The cell would hence experience less exposure to the field post-permeabilization, and both permeabilization and delivery would more likely decrease in this case.

Another charging time is the electrode screening time,

$$\tau_c = \frac{\lambda_D L}{D},$$

where λ_D is the Debye thickness for the electrical double layer, L is the distance between the electrodes, and D is a characteristic ion diffusivity [63]. This time scale is calculated with a resistor–capacitor model. For electroporation experiments, it characterizes the time for significant field reduction to occur due to ion accumulation near the electrodes. Using $\lambda_D=3$ nm (for typical buffer with an ion concentration around 10 mM), $L=1$ mm, and $D=10^{-9}$ m^2/S, τ_c is on the order of 3 ms, much longer in general than the pulsing time in both [47] and [48]. This mechanism is therefore also unlikely responsible for the observed conductivity effects.

4.2. Membrane permeabilization and diffusion

In Müller et al. [48] the authors proposed that the conductivity-dependent electrodeformation force determines the degree of electropermeabilization, which in turn causes the observed dependence of delivery on the extracellular conductivity. The normal component of the electrical pressure acting on the membrane, P_D, is given by the formula:

$$P_D = \frac{9}{2}\int_w E_0^2\cos^2\theta\frac{\sigma_i^2-\sigma_e^2}{(\sigma_i+2\sigma_e)^2}, \tag{15}$$

where ϵ_w is the permittivity for an aqueous solution. We argue that this mechanism is neither likely a viable interpretation. Although Eq. (15) does have a similar dependence on σ_e through the denominator, the more conspicuous feature is that P_D depends on E_0^2, not E_0 as shown in the experiments. Indeed, a companion study by Zimmermann and co-authors and a recent work by us both indicate that deformation depends quadratically on E_0 [49,64]. However, we do not exclude the possibility that electropermeabilization *can* depend strongly on the conductivity, through unknown mechanisms not included in the current Krassowska–Neu framework. Furthermore, if such mechanisms do exist, the influence on delivery would more likely manifest itself through diffusion, not electrophoresis which tends not to be affected by permeabilization. (We have adequately argued this latter point in our previous work [50].)

In Section 3.1, our simulation indicates that diffusion contributes very little to the total delivery in the case studied, due to a rapid resealing of the pores post-pulsation. (Most pores disappear at around 200 ns accordingly to the model.) This effect, however, may be due to an under-prediction of the post-pulsation PAD and/or its persistence

time scale. Past work indicates that pore resealing occurs on the time scale of a few seconds to tens of minutes [65,66,55,67–69]. Furthermore, if diffusion affects transport appreciably, such as demonstrated by Pucihar et al. [53], the effects together can contribute to the data trend observed. Although our simulation shows that diffusion results in only a small portion of the total molecules delivered with nano-second pulses for the short duration simulated, over a long time it may have more significant contributions. Indeed, the importance of diffusion can be seen from various previous experiments [70,60,71,53,72]. In this case, if the post-pulsation PAD has a strong and inverse dependence on the extracellular conductivity, its effect will manifest through diffusive transport, and hence contribute to the overall trend observed. Further experiments as well as model development (to take into account the conductivity-dependent membrane forces) are needed to help quantify the effects of both permeabilization and transport, and are the scope of our on-going work.

4.3. Other experimental observations

In the current work we have focused on interpreting the data from the two papers by Zimmerman and co-authors [73,48]. Other experimental data exist in the literature, and sometimes provide contradicting trends. For example, Ivorra et al. [74] observed that if medium conductivity decreased then higher field strength was required to achieve the "same effects". Rols et al. [75] discovered that increasing the ionic strength of the pulsing medium resulted in an increase in sieving of transient permeant structures. These trends are opposite of those observed in [47,48], and cannot be readily captured by the current model without a detailed study. We speculate that these discrepancies may be attributed to the specific parametric configurations used in the respective experiments. For example, in [74], the very low electrical conductivity may bring about additional effects due to very thick electrical double layers both around the cell and next to the electrodes. This latter factor affects the distribution of the electric field significantly. However, for electroporation in the classical regime, our recent experiments indicate trends in agreement with those by Zimmerman and co-authors. These results are presented in a recent publication [76], and are not repeated here for brevity.

Meanwhile, our model prediction provides qualitative agreement with other experimental data in terms of membrane conductance. In Suzuki et al. [77] (Fig. 9 therein), the measured membrane was higher when the extracellular conductivity was increased. This correlation is correctly captured in Fig. 7 below. In fact, a positive correlation of the membrane conductance with extracellular conductivity is consistent with the dependence of membrane permeabilization on conductivity as presented in Fig. 2d. As we argued previously, the variation in conductance or permeability is not responsible for the variability in delivery as observed by the various authors.

4.4. Limitations of the current model

Inevitably, the current model is a significant idealization to the realistic physical configuration of the problem. First, the cell membrane is assumed to be a spherical shell with a given dielectric constant. In reality, a cell membrane contains bilayer molecules, protein, carbohydrates, among others. None of these effects are considered in the ASE model for membrane permeabilization. In addition, the model does not differentiate between supra and classical electroporation. In other words, it may not capture the fundamental differences in the membrane behavior when subjected to nano-second and longer pulses. Second, the cell cytoplasm is considered to be uniform. Here we neglect the organelles and assume that DNA molecules are uniformly distributed inside the cell. In contrast, a physical cell is heterogeneous, and most of the DNA binding sites are located inside the nucleus. Despite these simplifications, we expect the qualitative conclusions in this paper to hold. As we demonstrated previously [50] and in the current work, as long as the membrane is reasonably permeabilized, electrophoretic transport depends much less on the details of membrane permeabilization, but rather on the distribution of the heterogeneous electric field. Furthermore, the assumed uniformity in the binding sites within the cell would affect the specific distribution of the species concentration within the cell, but would have little effect on the total amount of delivery.

5. Conclusions

In this work we presented a model study of ion delivery into permeabilized cells. The model system combines the Neu–Krassowska framework for permeabilization with Nernst–Planck equations for ion transport, and is used to study the delivery of PI into mammalian cells following experiments by Müller et al. [48] and Djuzenova et al. [47]. The focus of the study is to provide mechanistic interpretations of the observed inverse correlations between delivery and the extracellular conductivity. Our main conclusions are as follows.

- Our results indicate that neither the transmembrane potential nor the membrane permeabilization depends strongly on the extracellular conductivity. Instead, the interplay between the two parameters drives them toward their respective equilibrium states.
- The conductivity does strongly affect the spatial distribution of the electric field, which in turn results in varied total delivery. The model successfully predicts an inverse correlation between the two parameters.
- The model results compare well with experimental observations in general, but yield a weaker correlation between extracellular conductivity and delivery. Satisfactory fitting curves on the data are obtained when modifying the predicted correlation with a constant. The success of the model suggests the importance of electrophoretic transport in mediating delivery. The discrepancy between the results suggests that an unknown mechanism not included in the current framework contributes to molecular transport. The cause of the discrepancy is currently being investigated.

Based on the simulation and a control volume analysis, we have developed a simple formula to predict electrophoresis-mediated ion delivery. The formula provides an accurate approximation to the results from the full model, and can be used as a compact, convenient formula in place of the more complex and costly simulations. Together this work is an important step toward the quantification of molecular delivery via electroporation.

Appendix A. Compact model for molecular delivery via electrophoresis

In this section, we develop a simplified and compact model to predict molecular delivery via electrophoretic transport. This development is based on the results from our previous work [50], where we find that the degree of permeabilization does not significantly affect transmembrane molecular flux. In fact, the effect of membrane permeabilization is rectified by ion accumulation or depletion around the polar caps, and the resulting flux into the cell mainly depends on the ambient conditions in the buffer. This finding allows us to significantly simplify the problem, such that a theoretical approximation can be derived to estimate molecular delivery.

As an idealization, we assume that the membrane is completely permeabilized, such that both the electric potential and the Ohmic current are continuous:

$$\Phi_i|_{r=a} = \Phi_e|_{r=a}, (\mathbf{n}\cdot\sigma_i\nabla\Phi_i)_{r=a} = (\mathbf{n}\cdot\sigma_e\nabla\Phi_e)_{r=a}. \tag{A.1}$$

This idealization ignores the presence of both a finite TMP and non-permeabilized areas on the membrane. However, it makes the analysis tractable, and provides a reasonable approximation to the

far-field electric field. The solution to Eq. (1) using the matching condition (A.1) gives:

$$\begin{cases} \Phi_e = -E_0\left(1+\lambda\frac{a^3}{r^3}\right)r\cos\theta \\ \Phi_i = -\frac{3\sigma_e}{2\sigma_e+\sigma_i}E_0 r\cos\theta \end{cases}, \tag{A.2}$$

where $\lambda \equiv (\sigma_e-\sigma_i)/(2\sigma_e+\sigma_i)$. The external electric field is then given as

$$\mathbf{E}_e(r) = E_0\left(1-2\lambda\frac{a^3}{r^3}\right)\cos\theta\mathbf{e}_r - E_0\left(1+\lambda\frac{a^3}{r^3}\right)\sin\theta\mathbf{e}_\theta.$$

A control volume is shown in Fig. A.8. The surface A_1 denotes a semi-sphere far away from the cell, $R \gg a$. The annular disk A_2 connects A_1 with the cell surface. We conveniently ignore diffusive transport and assume that the molecular concentration on these surfaces remains ambient (denoted by c_e). On each surface, the molecular flux density $\mathcal{F}_{\text{ep}}$ (per unit area) is computed as

$$\mathcal{F}_{\text{ep}} = -\mathbf{n}\cdot\mathbf{u}_{\text{ep}} \times c_e,$$

where $\mathbf{n}$ is the outward unit normal, and $\mathbf{u}_{\text{ep}} = -wFz\nabla\Phi$ is the electrophoretic velocity vector. The total flux into the cell is simply the influx through A_1 subtracting the efflux through A_2. A straightforward calculation reveals

$$\mathcal{F}_{\text{tot}} = c_e wFzE_0(t)\pi a^2\left(\frac{3\sigma_i}{2\sigma_e+\sigma_i}\right).$$

The total molecular delivery, c_{tot}, is the integration of the flux with respect to the time in the presence of an electric pulse. For a constant electric field with pulse length t_{pulse},

$$c_{\text{tot}} = t_{\text{pulse}} \times \left[c_e wFzE_0\pi a^2\left(\frac{3\sigma_i}{2\sigma_e+\sigma_i}\right)\right]. \tag{A.3}$$

In deriving Eq. (A.3) we also assume that the time for membrane permeabilization is negligible. However, the formula can be easily modified should this time become comparable to the total pulse length. Note that c_{tot} depends on the conductivities via the factor $3\sigma_i/(2\sigma_e+\sigma_i)$. This factor arises from the effect of intra- and extracellular conductivities on the electric field which is evidenced in Eq. (A.2).

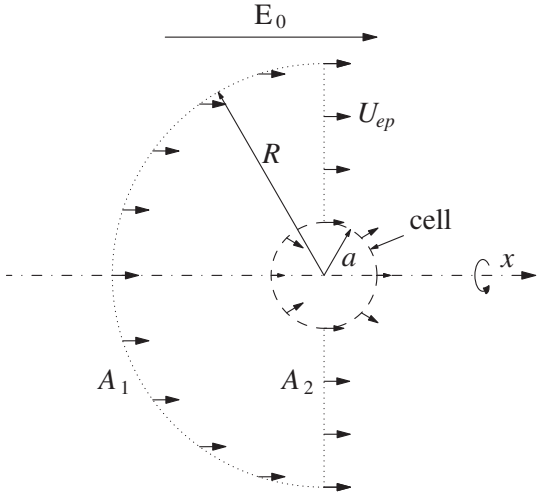

Fig. A.8. A control volume analysis for the total molecular flux into the cell. The control surface A_1 is semi-spherical and away from the cell. The annular disk A_2 connects A_1 and the cell surface. The flux into the cell is calculated by subtracting the efflux through A_2 from the influx through A_1. U_{ep} denotes electrophoretic velocity, and is the only mechanism considered for transport in the idealized analysis.

References

[1] L.M. Mir, Therapeutic perspectives of *in vivo* cell electropermeabilization, Bioelectrochemistry 53 (2000) 1–10.
[2] J. Gehl, Electroporation: theory and methods, perspectives for drug delivery, gene therapy and research, Acta Physiol. Scand. 177 (2003) 437–447.
[3] E. Neumann, M. Schaefer-Ridder, Y. Wang, P.H. Hofschneider, Gene transfer into electric fields mouse lyoma cells by electroporation in high electric field, EMBO J. 7 (1982) 841–845.
[4] In: E. Neumann, A.E. Sowers, C.A. Jordan (Eds.), Electroporation and Electrofusion in Cell Biology, Plenum Press, 1989.
[5] M. Bettan, M.A. Ivanov, L.M. Mir, F. Boissiere, P. Delaere, D. Scherman, Efficient DNA electrotransfer into tumors, Bioelectrochemistry 52 (2000) 83–90.
[6] M. Golzio, J. Teissié, M. Rols, Control by membrane order of voltage-induced permeabilization, loading and gene transfer in mammalian cells, Bioelectrochemistry 53 (2000) 25–34.
[7] G.T. Martin, U.F. Pliquett, J.C. Weaver, Theoretical analysis of localized heating in human skin subjected to high voltage pulses, Bioelectrochemistry 57 (2002) 55–64.
[8] U. Pliquett, R. Elez, A. Piiper, E. Neumann, Electroporation of subcutaneous mouse tumors by rectangular and trapezium high voltage pulses, Bioelectrochemistry 62 (2004) 83–93.
[9] U. Pliquett, T.S. Gallob, S.W. Huib, C. Gusbetha, E. Neumann, Local and transient structural changes in stratum corneum at high electric fields: contribution of joule heating, Bioelectrochemistry 67 (2005) 37–46.
[10] J. Teissié, M. Golzio, M.P. Rols, Mechanisms of cell membrane electropermeabilization: a minireview of our present (lack of ?) knowledge, Biochim. Biophys. Acta 1724 (2005) 270–280.
[11] J.M. Escoffre, T. Portet, L. Wasungu, J. Teissié, D. Dean, M.P. Rols, What is (still not) known of the mechanism by which electroporation mediates gene transfer and expression in cells and tissues, Mol. Biotechnol. 41 (2009) 286–295.
[12] A.O. Bilska, K.A. DeBruin, W. Krassowska, Theoretical modeling of the effects of shock duration, frequency, and strength on the degree of electroporation, Bioelectrochemistry 51 (2000) 133–143.
[13] C. Barrau, J. Teissié, B. Gabriel, Osmotically induced membrane tension facilitates the triggering of living cell electropermeabilization, Bioelectrochemistry 63 (2004) 327–332.
[14] S. Talele, P. Gaynorb, Non-linear time domain model of electropermeabilization: response of a single cell to an arbitrary applied electric field, J. Electrostat. 65 (2007) 775–784.
[15] D.C. Chang, T.S. Reese, Changes in membrane structure induced by electroporation as revealed by rapid-freezing electron microscopy, Biophys. J. 58 (1990) 1–12.
[16] H. Leontiadou, A.E. Mark, S.J. Marrink, Molecular dynamics simulations of hydrophilic pores in lipid bilayers, Biophys. J. 86 (2004) 2156–2164.
[17] D.P. Tieleman, The molecular basis of electroporation, BMC Biochem. 5 (2004) 10.
[18] A.A. Gurtovenko, I. Vattulainen, Pore formation coupled to ion transport through lipid membranes as induced by transmembrane ionic charge imbalance: atomistic molecular dynamics study, J. Am. Chem. Soc. 127 (2005) 17570–17571.
[19] M. Tarek, Membrane electroporation: a molecular dynamics simulation, Biophys. J. 88 (2005) 4045–4053.
[20] J. Wohlert, W.K. den Otter, O. Edholm, W.J. Briels, Free energy of a transmembrane pore calculated from atomistic molecular dynamics simulations, J. Chem. Phys. 124 (2006) 154905.
[21] U. Pliquett, R.P. Joshi, V. Sridhara, K.H. Schoenbach, High electrical field effects on cell membranes, Bioelectrochemistry 70 (2007) 275–282.
[22] M.L. Fernández, G. Marshall, F. Sagués, R. Reigada, Structural and kinetic molecular dynamics study of electroporation in cholesterol-containing bilayers, J. Phys. Chem. B 114 (2010) 6855–6865.
[23] Z.A. Levine, P.T. Vernier, Life cycle of an electropore: field-dependent and field-independent steps in pore creation and annihilation, J. Membr. Biol. 236 (2010) 27–36.
[24] V.F. Pastushenko, Y.A. Chizmadzhev, V.B. Arakelyan, Electric breakdown of bilayer lipid membranes II: calculation of the membrane lifetime in the steady-state diffusion approximation, Bioelectrochem. Bioenerg. 6 (1979) 53–62.
[25] A. Barnett, J.C. Weaver, Electroporation: a unified, quantitative theory of reversible electrical breakdown and rupture in artificial planar bilayer membranes, Bioelectrochem. Bioenerg. 25 (1991) 163–182.
[26] S.A. Freeman, M.A. Wang, J.C. Weaver, Theory of electroporation of planar bilayer membranes: prediction of the aqueous area, change in capacitance, and pore–pore separation, Biophys. J. 67 (1994) 42–56.
[27] K.A. Debruin, W. Krassowska, Modeling electroporation in a single cell. I. Effects of field strength and rest potential, Biophys. J. 77 (1999) 1213–1224.
[28] J.C. Neu, W. Krassowska, Asymptotic model of electroporation, Phys. Rev. E: Stat. Nonlinear Soft Matter Phys. 59 (1999) 3471–3482.
[29] R.P. Joshi, Q. Hu, K.H. Schoenbach, Dynamical modeling of cellular response to short-duration, high-intensity electric fields, IEEE Trans. Dielectr. Electr. Insul. 10 (2003) 778–787.
[30] D.A. Stewart, T.R. Gowrishankar, J.C. Weaver, Transport lattice approach to describing cell electroporation: use of a local asymptotic model, IEEE Trans. Plasma Sci. 32 (2004) 1696–1708.

[31] Z. Vasilkoski, A.T. Esser, T.R. Gowrishankar, J.C. Weaver, Membrane electroporation: the absolute rate equation and nanosecond time scale pore creation, Phys. Rev. E: Stat. Nonlinear Soft Matter Phys. 74 (2006) 021904.
[32] A.T. Esser, K.C. Smith, T.R. Gowrishankar, J.C. Weaver, Towards solid tumor treatment by irreversible electroporation: intrinsic redistribution of fields and currents in tissue, Technol. Cancer Res. Treat. 6 (2007) 261.
[33] W. Krassowska, P.D. Filev, Modeling electroporation in a single cell, Biophys. J. 92 (2007) 404–417.
[34] K.C. Smith, J.C. Weaver, Active mechanisms are needed to describe cell responses to submicrosecond, megavolt-per-meter pulses: cell models for ultrashort pulses, Biophys. J. 95 (2008) 1547–1563.
[35] M. Rols, J. Teissié, Electropermeabilization of mammalian cells to macromolecules: control by pulse duration, Biophys. J. 75 (1998) 1415–1423.
[36] J. Teissié, J.M. Escoffre, M.P. Rols, M. Golzio, Time dependence of electric field effects on cell membranes. A review for a critical selection of pulse duration for therapeutical applications, Radiol. Oncol. 42 (2008) 196–206.
[37] M.S. Venslauskas, S. Šatkauskas, R. Rodaitė-Riševičienė, Efficiency of the delivery of small charged molecules into cells *in vitro*, Bioelectrochemistry 79 (2010) 130–135.
[38] V.A. Klenchin, S.I. Sukharev, S.M. Serov, L.V. Chernomordik, Y.A. Chizmadzhev, Electrically induced DNA uptake by cells is a fast process involving DNA electrophoresis, Biophys. J. 60 (1991) 804–811.
[39] S.I. Sukharev, V.A. Klenchin, S.M. Serov, L.V. Chernomordik, Y.A. Chizmadzhev, Electroporation and electrophoretic DNA transfer into cells, Biophys. J. 63 (1992) 1320–1327.
[40] H. Wolf, M.P. Rols, E. Boldt, E. Neumann, J. Teissié, Control by pulse parameters of electric field-mediated gene transfer in mammalian cells, Biophys. J. 66 (1994) 524–531.
[41] M.F. Bureau, J. Gehl, V. Deleuze, L.M. Mir, D. Scherman, Importance of association between permeabilization and electrophoretic forces for intramuscular DNA electrotransfer, Biochim. Biophys. Acta 1474 (2000) 353–359.
[42] M. Golzio, J. Teissié, M. Rols, Direct visualization at the single-cell level of electrically mediated gene delivery, Proc. Natl. Acad. Sci. U. S. A. 99 (2002) 1292–1297.
[43] K.J. Müller, M. Horbaschek, K. Lucas, U. Zimmermann, V.L. Sukhorukov, Electrotransfection of anchorage-dependent mammalian cells, Exp. Cell Res. 288 (2003) 344–353.
[44] D.A. Zaharoff, J.W. Henshaw, B. Mossop, F. Yuan, Mechanistic analysis of electroporation-induced cellular uptake of macromolecules, Exp. Biol. Med. 233 (2008) 94–105.
[45] S. Haberl, D. Miklavčič, M. Pavlin, Effect of Mg ions on efficiency of gene electrotransfer and on cell electropermeabilization, Bioelectrochemistry 79 (2010) 265–271.
[46] M. Wu, F. Yuan, Membrane binding of plasmid DNA and endocytic pathways are involved in electrotransfection of mammalian cells, PLoS One 9 (2011) e20923.
[47] C.S. Djuzenova, U. Zimmermann, H. Frank, V.L. Sukhorukov, E. Richter, G. Fuhr, Effect of medium conductivity and composition on the uptake of propidium iodide into electropermeabilized myeloma cells, Biochim. Biophys. Acta 1284 (1996) 143–152.
[48] K.J. Müller, V.L. Sukhorukov, U. Zimmermann, Reversible electropermeabilization of mammalian cells by high-intensity, ultra-short pulses of submicrosecond duration, J. Membr. Biol. 184 (2001) 161–170.
[49] V.L. Sukhorukov, H. Mussauer, U. Zimmermann, The effect of electrical deformation forces on the electropermeabilization of erythrocyte membranes in low- and high-conductivity media, J. Membr. Biol. 163 (1998) 235–245.
[50] J. Li, H. Lin, Numerical simulation of molecular uptake via electroporation, Bioelectrochemistry 82 (2011) 10–21.
[51] M. Puc, T. Kotnik, L.M. Mir, D. Miklavčič, Quantitative model of small molecules uptake after *in vitro* cell electropermeabilization, Bioelectrochemistry 60 (2003) 1–10.
[52] K.C. Smith, J.C. Neu, W. Krassowska, Model of creation and evolution of stable electropores for DNA delivery, Biophys. J. 86 (2004) 2813–2826.
[53] G. Pucihar, T. Kotnik, D. Miklavčič, J. Teissié, Kinetics of transmembrane transport of small molecules into electropermeabilized cells, Biophys. J. 95 (2008) 2837–2848.
[54] Z. Rong, Bipartite expressions for diffusional mass transport in biomembranes, Biophys. J. 91 (2006) 4690–4696.
[55] R. Shirakashi, V.L. Sukhorukov, I. Tanasawa, U. Zimmermann, Measurement of the permeability and resealing time constant of the electroporated mammalian cell membranes, Int. J. Heat Mass Transfer 47 (2004) 4517–4524.
[56] Y. Granot, B. Rubinsky, Mass transfer model for drug delivery in tissue cells with reversible electroporation, Int. J. Heat Mass Transfer 51 (2008) 5610–5616.
[57] D. Miklavcic, L. Towhidi, Numerical study of the electroporation pulse shape effect on molecular uptake of biological cells, Radiol. Oncol. 44 (2010) 34–41.
[58] B. Gabriel, J. Teissié, Time courses of mammalian cell electropermeabilization observed by millisecond imaging of membrane property changes during the pulse, Biophys. J. 76 (1999) 2158–2165.
[59] J. Li, H. Lin, The current–voltage relation for electropores with conductivity gradients, Biomicrofluidics 4 (2010) 013206.
[60] V.L. Sukhorukov, C.S. Djuzenova, H. Frank, W.M. Arnold, U. Zimmermann, Electropermeabilization and fluorescent tracer exchange — the role of whole-cell capacitance, Cytometry 21 (1995) 230–240.
[61] W.D. Wilson, C.R. Krishnamoorthy, Y. Wang, J.C. Smith, Mechanism of intercalation: ion effects on the equilibrium and kinetic constants for the interaction of propidium and ethidium with DNA, Biopolymers 24 (1985) 1941–1961.
[62] J. Deng, K.H. Schoenbach, E.S. Buescher, P.S. Hair, P.M. Fox, S.J. Beebe, The effects of intense submicrosecond electrical pulses on cells, Biophys. J. 84 (2003) 2709–2714.
[63] M.Z. Bazant, K. Thornton, A. Ajdari, Diffuse-charge dynamics in electrochemical systems, Phys. Rev. E: Stat. Nonlinear Soft Matter Phys. 70 (2004) 021506.
[64] M.M. Sadik, J. Li, J.W. Shan, D.I. Shreiber, H. Lin, Vesicle deformation and poration under strong dc electric fields, Phys. Rev. E: Stat. Nonlinear Soft Matter Phys. 83 (2011) 066316.
[65] J.C. Weaver, Y.A. Chizmadzhev, Theory of electroporation: a review, Bioelectrochem. Bioenerg. 41 (1996) 135–160.
[66] M. Schmeer, T. Seipp, U. Pliquett, S. Kakorin, E. Neumann, Mechanism for the conductivity changes caused by membrane electroporation of CHO cell-pellets, Phys. Chem. Chem. Phys. 6 (2004) 5564–5574.
[67] M. Pavlin, M. Kandušer, M. Reberšek, G. Pucihar, F.X. Hart, R. Magjarević, D. Miklačič, Effect of cell electroporation on the conductivity of a cell suspension, Biophys. J. 88 (2005) 4378–4390.
[68] M. Kandušer, M. Šentjurc, D. Miklavčič, Cell membrane fluidity related to electroporation and resealing, Eur. Biophys. J. 35 (2006) 196–204.
[69] A.G. Pakhomov, A.M. Bowman, B.L. Ibey, F.M. Andre, O.N. Pakhomova, K.H. Schoenbach, Lipid nanopores can form a stable, ion channel-like conduction pathway in cell membrane, Biochem. Biophys. Res. Commun. 385 (2009) 181–186.
[70] M.R. Prausnitz, J.D. Corbett, J.A. Gimm, D.E. Golan, R. Langer, J.C. Weaver, Millisecond measurement of transport during and after an electroporation pulse, Biophys. J. 68 (1995) 1864–1870.
[71] E. Neumann, K. Toensing, S. Kakorin, P. Budde, J. Frey, Mechanism of electroporative dye uptake by mouse B cells, Biophys. J. 74 (1998) 98–108.
[72] S.M. Kennedy, Z. Ji, J.C. Hedstrom, J.H. Booske, S.C. Hagness, Quantification of electroporative uptake kinetics and electric field heterogeneity effects in cells, Biophys. J. 94 (2008) 5018–5027.
[73] C.S. Djuzenova, V.L.S.G. Klöck, W.M. Arnold, U. Zimmermann, Effect of electric-field pulses on the viability and on the membrane-bound immunoglobulins of LPS-activated murine B-lymphocytes — correlation with the cell-cycle, Cytometry 15 (1994) 35–45.
[74] A. Ivorra, J. Villemejane, L.M. Mir, Electrical modeling of the influence of medium conductivity on electroporation, Phys. Chem. Chem. Phys. 12 (2010) 10055–10064.
[75] M. Rols, J. Teissié, Electropermeabilization of mammalian cells to macromolecules: control by pulse duration, Biophys. J. 75 (1989) 1415–1423.
[76] M.M. Sadik, J. Li, J.W. Shan, D.I. Shreiber, H. Lin, Quantification of ion transport during electroporation-mediated molecular delivery, Biophys. J. (submitted for publication).
[77] D.O.H. Suzuki, A. Ramos, M.C.M. Ribeiro, L.H. Cazarolli, F.R.M.B. Silva, L.D. Leite, J.L.B. Marques, Theoretical and experimental analysis of electroporated membrane conductance in cell suspension, IEEE Trans. Biomed. Eng. 58 (2011) 3310–3318.